THE ASTROPHYSICAL JOURNAL, 235:11–17, 1980 January 1

THE MILLI-ARCSECOND STRUCTURE OF 3C 147 AND 3C 380 DETERMINED BY HYBRID MAPPING WITH A FIVE-STATION ARRAY

A. C. S. READHEAD AND P. N. WILKINSON
California Institute of Technology
Received 1979 May 24; accepted 1979 July 17

ABSTRACT

Hybrid maps of 3C 147 and 3C 380 have been made from VLBI observations at 1671 MHz on a five-station network. The amount of amplitude and closure phase data is roughly double that obtained on four station networks, making these the most accurate and detailed maps of the milli-arcsecond structure of quasars that have yet been made. The morphologies of the sources are discussed briefly in the context of the beam model.

Subject headings: interferometry — quasars

I. INTRODUCTION

Recent tests (Readhead and Wilkinson 1978) have shown that it is possible to make reliable "hybrid" maps of radio sources from VLBI observations on four or more telescopes, when the closure phase is used in addition to the interferometer fringe amplitudes (Jennison 1958; Rogers *et al.* 1974).

The technique has been applied successfully to four-station observations at 609 MHz, 5011 MHz, and 10651 MHz (Wilkinson *et al.* 1977; Readhead *et al.* 1979; Wilkinson *et al.* 1979). In this paper we present new hybrid maps of 3C 147 and 3C 380 made from five-station observations at 1671 MHz. These maps, made from observations on 10 baselines and with six independent closure phase relations, represent by far the best determinations of the milli-arcsecond structure of extragalactic radio sources that have been made thus far. The maps are discussed briefly in the context of the beam model for the formation of extragalactic radio sources.

II. THE FIVE-STATION OBSERVATIONS AND HYBRID MAPS OF 3C 147 AND 3C 380

On 1976 September 28 and 29 we observed 3C 147 and 3C 380 at 1671 MHz on a five-station VLB network. Details of the stations are given in Table 1. The observations were made using the standard NRAO Mk II VLBI system (Clark 1973), and processed on the CIT–JPL processor at the California Institute of Technology. A number of calibration sources was also observed, and the calibration of the data was done by the standard technique (e.g., Cohen *et al.* 1977). We believe that systematic errors in the final amplitudes are less than 10%. Hybrid maps of 3C 147 and 3C 380 were made by the procedure described by Wilkinson *et al.* (1977), and by Readhead and Wilkinson (1978).

a) 3C 147

In the case of 3C 147 two maps have been made: one of the core alone, with a resolution of 2.4 milli-arcsec, and one of the core plus jet, with a resolution of 9 milli-arcsec. This was necessary because the sensitivity of the system did not permit us to use the maximum resolution on the low surface brightness jet, but the higher resolution is needed to show the details of the core. These two maps are shown in Figures 1*a* and 1*b*, and the fit of the delta functions to the data is shown in Figure 1*c*. The map (Fig. 1*a*) is also shown in the "radio photograph" (Fig. 2 [Pl. 1]). In this plate the core has been overexposed to make visible the details of the jet (see legend to Fig. 2).

The core (Fig. 1*b*) is basically a double source surrounded by a roughly circular low-surface-brightness region. The separation of the double is 3 milli-arcsec in position angle 53°. The double nature of

TABLE 1

INTERFEROMETER ELEMENTS

Location	Institution	Diameter (m)	T_{sys} (K)	T_{ant} (K Jy^{-1})
Effelsberg, W. Germany	Max Planck Institute (MPIR)	100	105	1.3
Greenbank, WV	NRAO	43	60	0.25
Ft. Davis, Texas (FDVS)	Harvard University	26	115	0.085
Big Pine, CA (OVRO)	Caltech	40	85	0.21
Hat Creek, CA (HCRK)	University of California, Berkeley	26	260	0.085

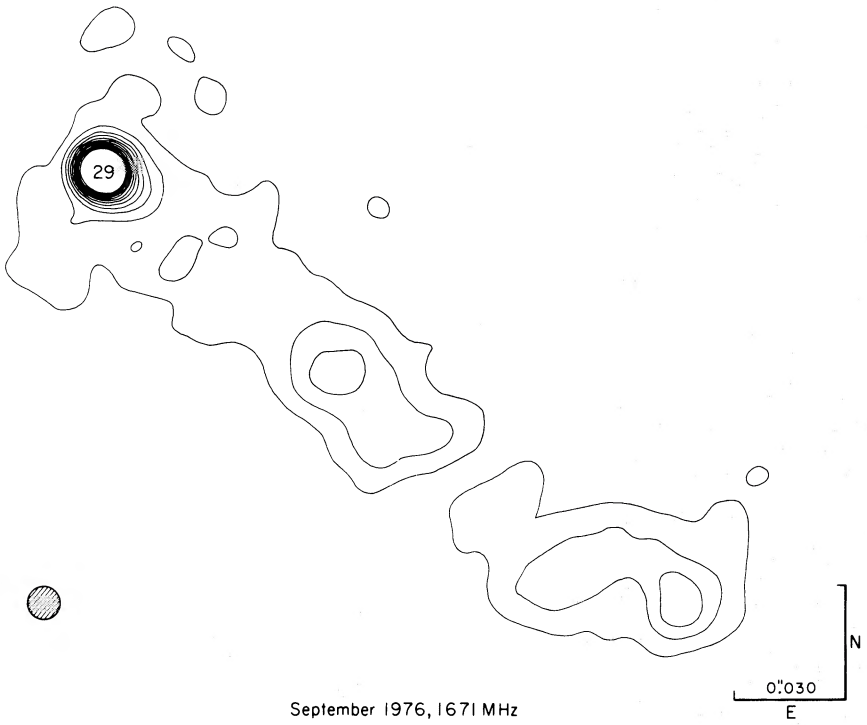

FIG. 1*a*.—Hybrid map of 3C 147. Restoring beam 0".009 × 0".009. Contour levels: 2, 6, 10, 14, . . . , 114 × 10^8 K.

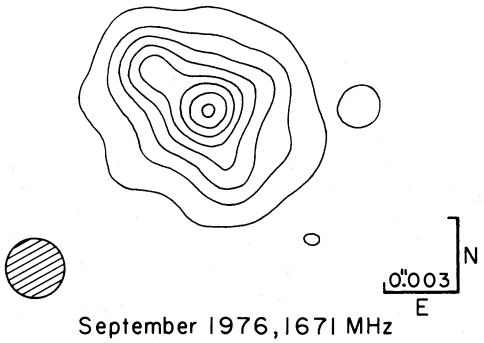

FIG. 1*b*.—Hybrid map of the core of 3C 147. Restoring beam 0".0024 × 0".0024. Contour levels: 4, 12, 20, . . . , 60 × 10^9 K.

the core is clear from the amplitude and closure phase data on the longer baselines, i.e., those involving MPIR, as can be seen in Figure 1*c*. It is not as clear that the core is a double in the hybrid map (Fig. 1*b*) because the restoring beam is comparable with the separation of the two components. The position angle of the core double is the same as that of the jet shown in Figure 1*a*, but different from the large-scale (0".5) structure seen by Donaldson and Smith (1971). We return to this point in § III.

The deep minima in correlated flux density in the interval GST 12^h–13^h5 on the HCRK–, OVRO–, and FDVS–MPIR baselines are due to beating between the two core components. Therefore the visibility phases on these three baselines flip through ~180° in this interval. The sign of the phase change depends on the exact ratio of flux densities in the two components. Thus, at a deep minimum, a very small error in this ratio can produce very discrepant visibility phases, and it should perhaps be emphasized that uncertainty in the exact phase behavior at a deep minimum has very little effect on the final map. In the present case the direction of flip in the closure phases was found to vary between maps which showed no significant differences. We have therefore left gaps in the fits wherever the closure phase of the map is not well determined.

A comparison of the map (Fig. 1*a*) of 3C 147 made at 1671 MHz with our previous map (Wilkinson *et al.* 1977) at 609 MHz, allows us to determine the spectral index α (defined as $S \propto \nu^{\alpha}$) of various features in this map. In Figure 3 we show cross-cuts through the source at p.a. −127° at the two frequencies. The scaling of the cuts has been chosen such that the curves intersect at $\alpha = -0.3$. Since the absolute position of the source is not recoverable from the closure phase, there is some uncertainty about the relative positions of the two maps. This point has been discussed in detail by Readhead *et al.* (1979). By applying similar arguments in the present case we find that, provided no part of the core (marked A in Fig. 3) has spectral index $\alpha < -1.5$, the relative positions of the two maps are fixed to within ±2.5 milli-arcsec.

A comparison of the 609 MHz and the 1671 MHz maps shows that over much of the jet $\alpha \sim -0.5$.

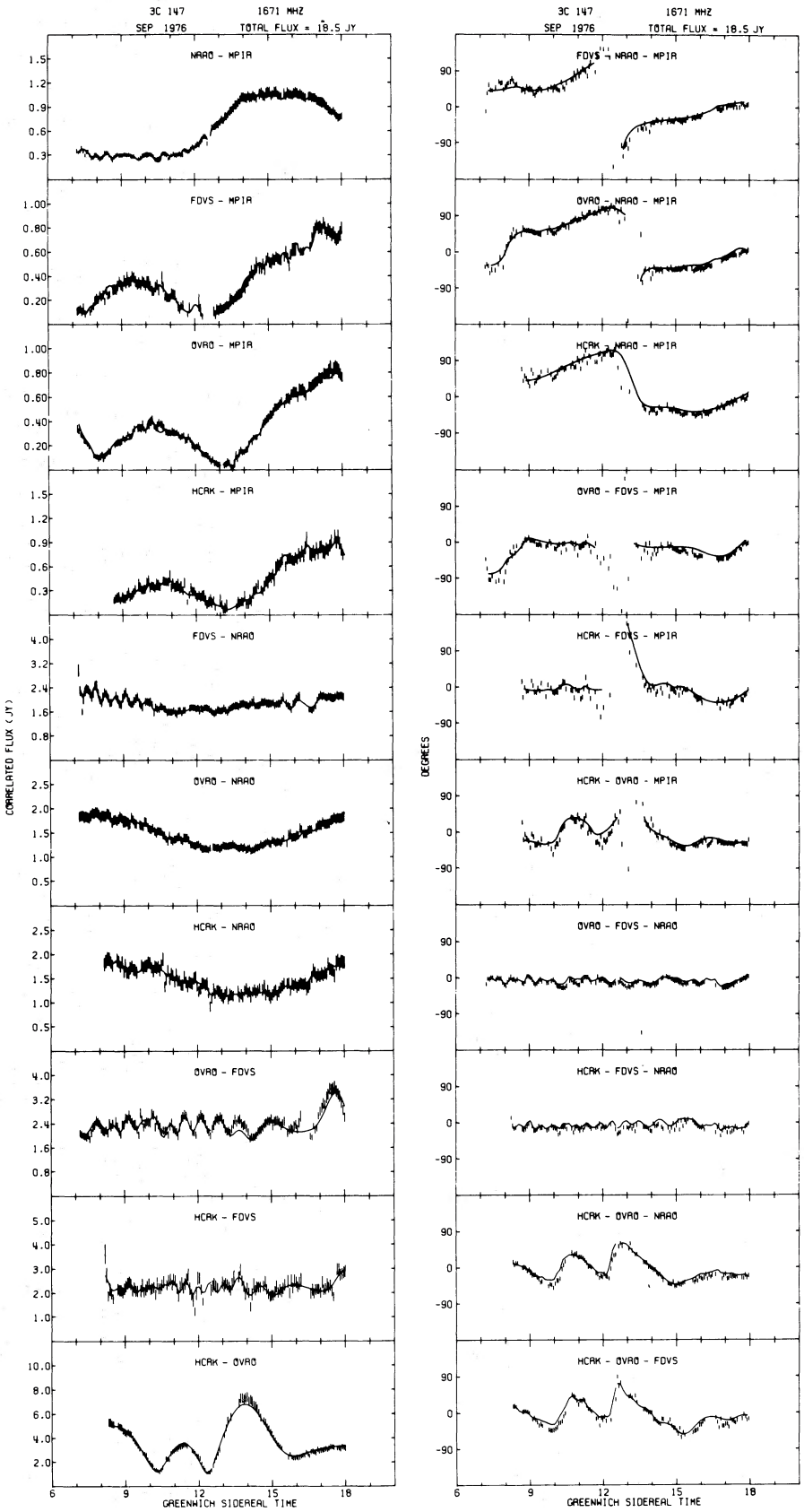

FIG. 1*c*.—The fit, to the observed amplitudes and closure phases, of the array of point sources, which are the basis of the hybrid map of Figs. 1*a* and 1*b*.

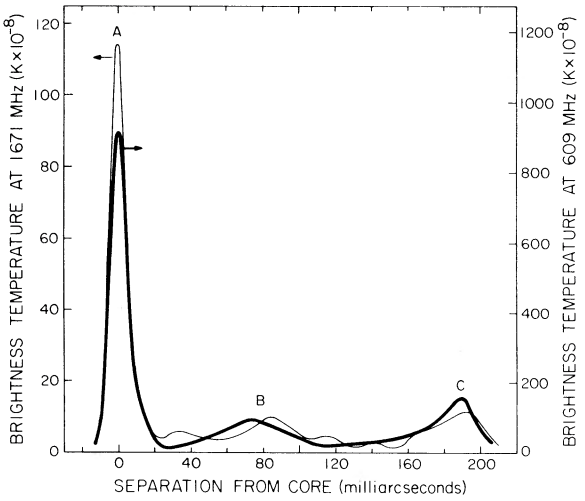

FIG. 3.—Profile of 3C 147 at 609 MHz and 1671 MHz, along cuts in p.a. −127°. The scales are chosen such that the curves intersect at $\alpha = -0.3$.

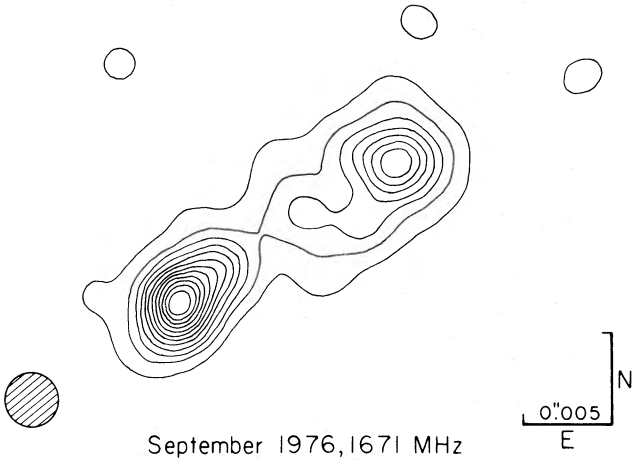

FIG. 4*a*.—Hybrid map of 3C 380. Restoring beam 0".003 × 0".003. Contour levels: 18, 54, 90, . . . , 414 × 10^8 K.

However, the cuts in Figure 3 are along the central ridge of the jet, and in these higher surface brightness features the spectral index is greater. In both the knots B and C the peak of emission is slightly farther from the core at the higher frequency. On the edges of the knots farther from the core the spectra are flatter ($\alpha > -0.3$), while on the nearer edges they are steeper ($\alpha < -0.3$). This trend is similar to that found on a much larger scale in many extragalactic radio sources, in which the outer edges of the outer components have flatter spectra than the trailing edges. Thus, by analogy, a plausible explanation of these effects in 3C 147 is that the core A is the center of activity and that the knots B and C are moving away from the core. The fact that the higher surface brightness features have flatter spectra suggests that synchrotron self-absorption might be responsible for most of the variations in spectral index. The same effect has also been observed in 3C 273 and 3C 345 (Readhead *et al.* 1979).

b) 3C 380

The hybrid map of 3C 380 is shown in Figure 4*a*. The delta functions which constitute this map give an excellent fit to the data. However, there are residual high-frequency modulations on the shorter baselines in both the closure phases and the amplitudes, which show that there are more distant components of 3C 380 which cannot be mapped from the present observations due to insufficient (u, v) coverage. The position of the brightest of these distant components can be determined unambiguously from the modulation in the amplitude and closure phase, and the limits which can be placed on its size and flux density are given in Table 2. This distant component has been added to the delta functions in the fit shown in Figure 4*b*. The separation in Table 2 is measured relative to the brighter (SE) component, which we assume to be the core of this object. In deriving these limits we have assumed that the distant component has a circular Gaussian brightness distribution. This is the most distant compact (<0".1) feature yet seen in any of the sources we have mapped. It could be a knot similar to knot C in 3C 147, which is at a distance of 0".2 from the core. Thus it would be interesting to map 3C 380 with lower resolution than the present observations, to see if there is a jet in this source similar to the one in 3C 147.

The source 3C 380 has also been mapped with the Cambridge 5 km telescope at 15 GHz, with a resolution of 0".7 (Scott 1977). At this resolution it is a double source with separation 1".2. The optical object coincides with the brighter (SE) component, and this is almost certainly the same component which we see in VLB observations. Based on this assumption we show the relative dispositions of the components in Figure 4*c*.

III. DISCUSSION

In a recent paper Readhead *et al.* (1978) have shown that the radio structure of nuclear components in extragalactic radio sources is strongly correlated with the morphology, distance, and overall size of the objects. They divide extragalactic radio sources into two types based on the morphology of the radio components. Objects in which the dominant radio emission is from two lobes, one on either side of the optical object, are called "symmetric" or Type S

TABLE 2

THE DISTANT COMPACT COMPONENT OF 3C 380

Separation from core	0".73 ± 0".01
Position angle	−50° ± 2°
Flux density	0.35 Jy < S < 10 Jy
Angular diameter (FWHM)	0".025 < θ < 0".075

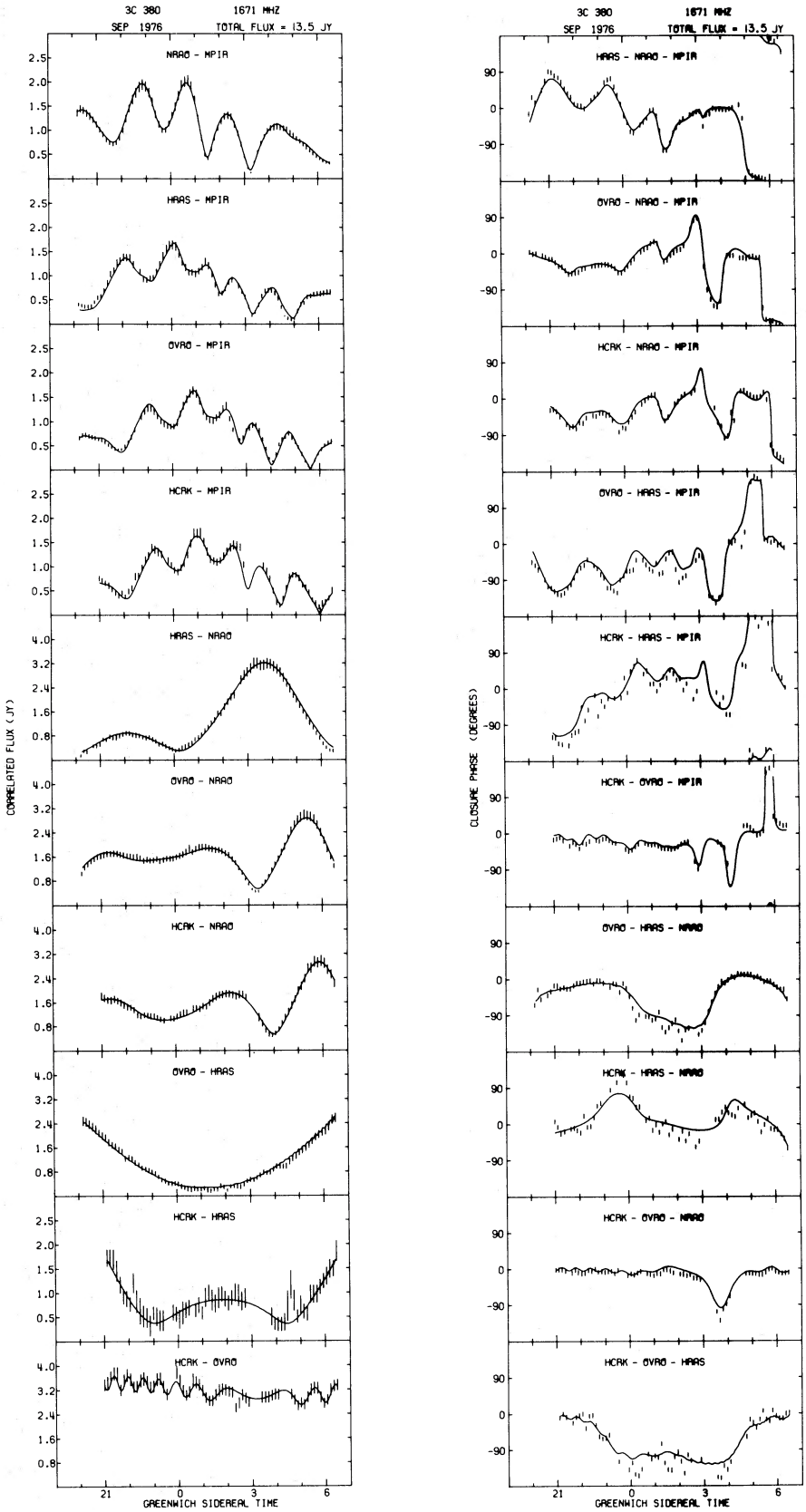

FIG. 4*b*.—The fit, to the observed amplitudes and closure phases, of the array of point sources, which are the basis of the hybrid map of Fig. 3*a*. The distant component (see text) has also been included.

objects. Objects which have a dominant radio component coincident with the optical object, and in which the extended structure, if any, is one-sided are called "core" or Type C objects. Readhead *et al.* (1978) have recently suggested a simple model which explains the gross differences between the two types of objects. On this model, most extragalactic radio sources consist of a center of activity which emits two highly collimated antiparallel beams, along which the particles move with relativistic bulk velocity, v. The regions of interaction between the beams and the intergalactic medium give rise to two extended ($>0''.1$) outer components which advance through the intergalactic medium with subrelativistic speeds ($\sim 0.03c$) and which radiate isotropically (Mackay 1973). The major differences between the core and symmetric objects are ascribed to different angles between the line of sight and the beam. In core objects this angle is small ($<1/\gamma$, where $\gamma = [1 - (v/c)^2]^{-1/2}$), and relativistic beaming of the radiation almost along the line of sight accounts for the apparent dominance of the central radio component. In symmetric objects the angle between the beam and the line of sight is larger ($>1/\gamma$) and the outer components dominate. On this model we expect to see extended components ($>0''.1$) in core objects too, but due to projection these will be superposed on the core components. In many core objects these extended regions would be difficult to detect in the presence of the strongly beamed core component.

The sources 3C 147 and 3C 380 are of particular interest to this discussion since they are both core objects, but they have steep ($\alpha < -0.7$) overall radio spectra between 300 MHz and 5 GHz. At frequencies below ~ 5 GHz both sources are dominated by a steep-spectrum, extended ($\sim 1''$) emission region which is almost coincident on the sky with the core component. We suggest that in both objects the steep-spectrum component is simply an outer component, of the type seen in symmetric objects, but here seen projected against the core. In symmetric sources these outer components radiate isotropically, and the two components usually have comparable luminosities (Mackay 1971). Thus in 3C 147 and 3C 380 it is not clear whether the steep-spectrum component is in front of the core object or behind it, or indeed whether *both* regions contribute a significant fraction of the flux density of this component. Both 3C 147 and 3C 380 exhibit a range of position angles between the compact and extended features. in 3C 147 the jet (Fig. 1*a*) is slightly curved. In addition the more extended structure ($\sim 0''.7$) is found to have a position angle $\sim 25°$ (or 155°) different from that of the jet (Donaldson and Smith 1972). The jet of 3C 147 bears a remarkable resemblance to the jet in 3C 274, which is also bent at one end (Wilkinson 1974; Arp and Lorre 1976). The curvature in 3C 380 can be seen in Figure 5 by comparing the position angles of the double source in the nucleus and the two distant components. These have, respectively, position angles relative to the nucleus of $-57°$, $-50°$, and $-37°$. The possible significance of the different position angles in core objects is discussed elsewhere (Readhead *et al.* 1978; Scheuer and Readhead 1979).

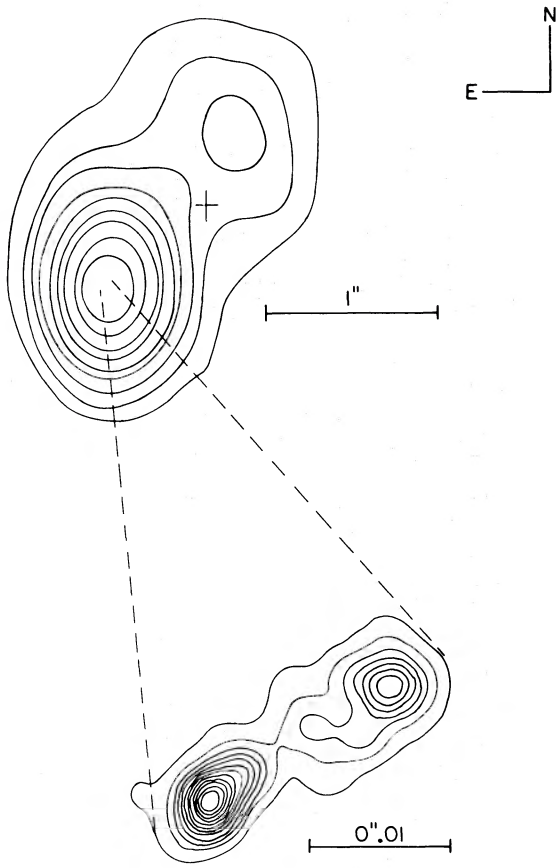

FIG. 5.—The relative disposition of the components of 3C 380; showing the nuclear double, and the larger-scale features of the Cambridge 5 km telescope map at 15 GHz (Scott 1977). The position of the distant component seen in the VLBI observations (see text) is marked with a cross.

The spectral indices determined in 3C 147 are of interest since, as is found in both 3C 273 and 3C 345 (Readhead *et al.* 1979), there are components with steep spectra near the nuclei of these quasars. Steep-spectrum components have not generally been detected in the nuclei of core objects because the spectrum of the nucleus is usually dominated by a bright component with a flat spectrum. However, we have seen that in 3C 147 the spectral index of the jet is $\alpha \sim -0.5$ between 609 MHz and 1671 MHz. Examination of the total spectrum, and decomposition of the spectrum into contributions from the three major components—core, jet, and halo—shows that the jet spectrum is flattened at 609 MHz, and therefore the high-frequency spectral index is steeper than the value $\alpha \sim -0.5$ found here (Wilkinson *et al.* 1977). In fact, at high frequencies $\alpha_{\rm jet} \sim -0.7$, i.e., the spectral index is similar to that which is observed in the extended outer components of many radio sources.

The spectral indices which we observed in different components of core objects have a natural explanation

in the beam model (Blandford and Rees 1974; Scheuer 1974; Blandford and Konigl 1979) if we assume that the electron injection spectrum is steep, and that this gives rise to a steep radio spectrum in all cases except in very high surface brightness features which are synchrotron self-absorbed. In these nuclei the higher surface brightness features have flat or inverted spectra (Readhead *et al.* 1979), whereas the low surface brightness features have steep spectra, just like the more extended features in the outer radio lobes of many radio sources.

Synchrotron self-absorption is the most plausible explanation for the flatter spectra of the core and knots (Wilkinson *et al.* 1977). Referring to Figure 3, there are unresolved features in the core (A) at both 1671 MHz and 609 MHz. Thus, at the lower frequency, $T_b > 10^{11}$ K so that synchrotron self-absorption would occur in magnetic fields $\sim 10^{-2}$ gauss. The brightness temperatures in the knots (B and C) are much lower, but the full resolution map shows that both of these knots contain compact unresolved regions in which the brightness temperatures are considerably higher than are shown here. Thus it is likely that synchrotron self-absorption in the presence of reasonable ($\sim 10^{-2}$ gauss) magnetic fields is responsible for the flatter spectra of the knots as well as the core.

Many of the sources which we have mapped have the same general morphology as 3C 147; i.e., there is a bright core at one end of a radio jet. This type of morphology is expected in the beam model if we identify the bright radio core, in each case, with the source of the beam, and the linear, jetlike, feature with the beam itself. The knots could be regions where enhanced turbulence gives rise to increased randomization of the bulk velocity of the matter in the beam, and hence to more radio emission. Such enhancements in the turbulence could occur as a result of the dynamics of the matter in the beam itself (e.g., Rees 1978) or because of increased interaction between the beam and interstellar matter (e.g., Blandford and Konigl 1978). It should be possible to distinguish between these two alternatives by asymmetries in the shape of the knots (Blandford and Konigl 1979). If the knots, B and C, are due to interactions between the beam and interstellar clouds, the steepest radio contour should face the core, A; whereas if they are due to propagating shocks within the beam itself, the steepest contours could be on either side of the knot. Inspection of Figure 1*a* shows that in knot B the steepest contours face the core whereas in knot C the reverse is true. The widths of the knots are comparable with the width of the jet. This is seen most clearly in maps of the jet with the full resolution (3 milli-arcsec) of the present observations. Furthermore, the observed spectra (Fig. 1*c*) show that in both knots B and C the trailing edges, i.e., the edges facing the core, have steep spectra, while the leading edges have flatter spectra. These effects suggest that any shocked regions associated with the knots extend across the width of the beam at the leading edges of the knots. This evidence is not conclusive, but it does favor the hypothesis that the knots are caused by shocks propagating in the beam, rather than interaction with interstellar clouds.

We are grateful to I. I. K. Pauliny-Toth and D. C. Backer for their help with the observations, to the Image Processing Laboratory of the Jet Propulsion Laboratory, Earth Resources Application Group, for making the radio photograph of 3C 147 from the hybrid map, to T. J. Pearson for his help with the data analysis, and to R. D. Blandford for useful discussions. Both of us are indebted to the Royal Society for Research Fellowships supported by the Weir Foundation during part of the time at which this work was carried out.

The National Radio Astronomy Observatory is operated under Associated Universities, Inc., under contract with the National Science Foundation. The work at Caltech is supported under National Science Foundation grants AST 77-22963 and AST 77-00247.

REFERENCES

Arp, H., and Lorre, J. 1976, *Ap. J.*, **210**, 58.
Blandford, R. D., and Rees, M. J. 1974, *M.N.R.A.S.*, **169**, 395.
Blandford, R. D., and Konigl, A. 1979, *Ap. J.*, in press.
Clark, G. G., 1973, *Proc. IEEE*, **61**, 1242.
Cohen, M. H., *et al.* 1977, *Nature*, **268**, 405.
Donaldson, W., and Smith, H. 1971, *M.N.R.A.S.*, **151**, 253.
Jennison, R. C. 1958, *M.N.R.A.S.*, **118**, 276.
MacKay, C. D. 1971, *M.N.R.A.S.*, **154**, 209.
———. 1973, *M.N.R.A.S.*, **162**, 1.
Readhead, A. C. S., Cohen, M. H., Pearson, T. S., and Wilkinson, P. N. 1978, *Nature*, **276**, 768.
Readhead, A. C. S., Pearson, T. J., Cohen, M. H., Ewing, M. S., Moffet, A. T. 1979, *Ap. J.*, **231**, 299.
Readhead, A. C. S., and Wilkinson, P. N. 1978, *Ap. J.*, **223**, 25.
Rogers, A. E. E., *et al.* 1974, *Ap. J.*, **193**, 293–301.
Scheuer, P. A. G. 1974, *M.N.R.A.S.*, **166**, 329.
Scheuer, P. A. G., and Readhead, A. C. S. 1979, *Nature*, **277**, 182.
Scott, M. A. 1977, *M.N.R.A.S.*, **179**, 377.
Wilkinson, P. N. 1974, *Nature*, **252**, 661.
Wilkinson, P. N., Readhead, A. C. S., Anderson, B., and Purcell, G. H. 1979, *Ap. J.*, in press.
Wilkinson, P. N., Readhead, A. C. S., Purcell, G. H., and Anderson, B. 1977, *Nature*, **209**, 764.

A. C. S. READHEAD: California Institute of Technology, Owens Valley Radio Observatory, Mail Code 102-24, Pasadena, CA 91125

P. N. WILKINSON: Nuffield Radio Astronomy Laboratory, Jodrell Bank, Cheshire, England

FIG. 2.—"Radio photograph" from hybrid map of Fig. 1*a*. The source has been rotated counterclockwise by 35°. The brightness temperature was scaled to produce numbers in the range 1 to 128, and the three most significant bits were then clipped. This gives the full range of the gray scale (16 levels) to the features in the jet, and produces the dark rings in the core. Thus the brightest features in the jet are about one eighth of the peak brightness of the core, and the successive dark rings are contours at one, two, . . . , etc., eighths of the peak core brightness.